Taylor & Francis
Taylor & Francis Group

ORIGINAL RESEARCH

🔓 OPEN ACCESS Check for updates

Regional immune mechanisms enhance efficacy of an autologous cellular cancer vaccine with intraperitoneal administration

Ben Marwedel[a], Lorél Y. Medina[a], Henning De May[b], Joshua E. Adogla[a], Ellie Kennedy[a], Erica Flores[a], Eunju Lim[a], Sarah Adams[b], Eric Bartee[a], and Rita E. Serda[a]

[a]Internal Medicine, University of New Mexico Health Science Center, Albuquerque, NM, USA; [b]Department of Obstetrics & Gynecology, University of New Mexico Health Science Center, Albuquerque, NM, USA

ABSTRACT

Widespread peritoneal dissemination is common in patients with gynecologic or gastrointestinal cancers. Accumulating evidence of a central role for regional immunity in cancer control indicates that intraperitoneal immunotherapy may have treatment advantages. This study delineates immune mechanisms engaged by intraperitoneal delivery of a cell-based vaccine comprised of silicified ovarian cancer cells associated with enhanced survival. Vaccine trafficking from the site of injection to milky spots and other fat-associated lymphoid clusters was studied in syngeneic cancer models using bioluminescent and fluorescent imaging, microscopy, and flow cytometry. Spectral flow cytometry was used to phenotype peritoneal immune cell populations, while bioluminescent imaging of cancer was used to study myeloid and T cell dependency, systemic immunity, and vaccine efficacy in models of disseminated high-grade serous ovarian and DNA mismatch-repair proficient microsatellite-stable colorectal cancer. Following intraperitoneal vaccination of mice with ovarian cancer, vaccine cells were rapidly internalized by myeloid cells, with subsequent trafficking to fat-associated lymphoid clusters. Tumor clearance was confirmed to be T cell-mediated, leading to the establishment of local and systemic immunity. Combination immune checkpoint inhibitor and vaccine therapy in mice with advanced disease, characterized by an established suppressive tumor microenvironment, increased the number of mice with non-detectable tumors, however, change in tumor burden compared to vaccine monotherapy was not significant. Vaccination also resulted in tumor clearance in mouse models of metastatic colorectal cancer. This study demonstrates that intraperitoneal vaccine delivery has the potential to enhance vaccine efficacy by activating resident immune cells with the subsequent establishment of protective systemic anti-tumor immunity.

Introduction

We recently reported that cryo-silicified cancer cells can be used as a modular platform for highly effective personalized immune therapy.[1,2] The thin, hydroxylated silicified cell surface enables modification with immunogenic molecules, including microbial based Toll-like receptor (TLR) agonists. These ligands activate signaling pathways in immune cells via TLRs present both on and within immune cells.[3,4] Combination TLR4 and TLR9 activation restores antigen presenting functions of human ascites myeloid cells.[5] When used as a cellular vaccine, TLR agonist-decorated silicified tumor cells achieved tumor clearance in mice with small volume disseminated disease and induced protective immune memory resulting in long-term disease-free survival. In these studies, intraperitoneal delivery was critical to achieving durable disease control in advanced models of high-grade ovarian cancer, suggesting that activation of resident immune cells can overcome treatment limitations attributed to the immune suppressive tumor microenvironment.[2] Importantly, intraperitoneal treatment was also able to induce systemic immunity to control extraperitoneal disease. These results present a strategy to engage regional immune networks to optimally deploy a novel and highly effective personalized cancer vaccine.[6–8]

Ovarian, gastric, colorectal, pancreatic, and appendicular cancers are those most prone to peritoneal metastasis, with preferential tropism to the omentum.[9] The omentum, protective adipose tissue with a double layer of mesothelial cells, is characterized by the presence of milky spots.[10] Milky spots are clusters of immune cell aggregates on the periphery of the adipose tissue band.[11] Similar fat-associated lymphoid clusters (FALCs) are located in mesentery and gonadal fat.[9] Regional immune surveillance includes filtration of peritoneal fluid through milky spots and immune cell trafficking through the omentum, with rapid efflux into peritoneal fluid.[12–15] Following TLR4 activation, myeloid cells migrate to lymphoid clusters.[16,17] Fibroblastic reticular cells in milky spots provide additional immune support by secreting CCL19 and recruiting naïve lymphocytes in response to TLR agonists or inflammatory signals.[18] Thus, regional FALCs are specialized to interact with cells in the peritoneal cavity to regulate local immune responses.

In the setting of peritoneal carcinomatosis, tumor-associated CD8^{+} T cells become exhausted as cancer progresses,

contributing to the failure of tumor specific immunity.[19] This decrease in T cell functional capacity is associated with upregulation of PD-1 by peritoneal CD8^{+} T cells, as well as deficient CD28 co-stimulation by antigen presenting cells in human ovarian cancer.[20–22] Accumulating evidence demonstrates that immune clusters in non-lymphoid tissues regulate cancer immunity and impact disease outcomes. Zhang et al. reported that the presence of tertiary lymphoid structures (TLS) is associated with clinical response to checkpoint blockade therapy and improved clinical prognosis in high-grade serous ovarian cancer patients.[23] Furthermore, high-grade serous ovarian cancer patients with a high presence of TLS have greater immune infiltration and a higher tumor mutational burden score than patients with low TLSs.[23] Therapies that engage these localized immune networks would be expected to enhance anti-tumor immunity and disease control.

Here, we demonstrate that intraperitoneal administration of a cell-based cancer vaccine results in myeloid cell uptake and trafficking to FALCs, generating a highly effective adaptive T cell response and both local and systemic tumor immunity. Importantly, this approach achieved tumor clearance in models of high-grade ovarian cancer as well as advanced colorectal cancer, indicating the potential for broad clinical impact across tumor types.

Materials and methods

Materials

To functionalize silicified cells, CpG Oligonucleotide 1826 was purchased from Invivogen (San Diego, CA, USA), MPLA from Salmonella enterica serotype from Sigma (St. Louis, MO, USA), 25k linear PEI from Polysciences (Warrington, PA, US), and cell culture grade endotoxin free water from GE Healthcare (Chicago, IL, USA). Tetramethyl orthosilicate (TMOS), hydrochloric acid bioreagent, sodium chloride, puromycin dihydrochloride, and 10% buffered formalin were purchased from Sigma-Aldrich (St. Louis, MO, USA). Prolong™ Gold Antifade Mountant with DAPI, and phosphate-buffered saline (PBS) were purchased from Thermo Fisher Scientific (Waltham, MA, USA). Fetal bovine serum (FBS) was purchased from ATCC (Manassas, VA, USA). 0.05% EDTA trypsin solution and penicillin-streptomycin were purchased from Life Technologies Corporation (Carlsbad, CA, USA). Dulbecco's Modified Eagle's Medium (DMEM) was purchased from Caisson Labs (Smithfield, UT, USA). D-Luciferin Potassium Salt was purchased from Perkin Elmer (Boston, MA, USA).

Antibodies

Anti-CD11b antibody (clone M1/70, BD Bioscience) was used for microscopy and flow cytometry identification of myeloid cell association with vaccine. High throughput flow cytometry used the following antibodies: Ly6C (HK1.4) BV421, Ly6G (1A8) Spark Blue 550, CD45 (30-F11) BV510, CD11b (M1/70) BV570, CD19 (6D5) BV605, NKp46 (29A1.4) BV650, CD8a (53–6.7) PerCP, CD4 (GK1.5) PE Fire 700, CD25 (PC61H1.2F3) PE-Cy5, CD69 (H1.2F3) PE-Cy7, CD49b (HMa2) Alexa 647, and Zombie NIR (live dead) from Biolegend; CD3 (500A2) Pac Blue, and F4–80 (T45-2342)

APC from BD Pharmingen; PD1 (CD279, J43) BV480 and NK1.1 (PK136) BV750 from BD Optibuild; and CD49a (Ha31/8) BV711, CD11c (HL3) BV786, and Tim3 (5D12/TIM-3) PECF549 from BD Horizon, and I-A (M5/114.15.2) Alexa 532 and B220 (RA3-6B2) APC Cy5.5 from Invitrogen. Flow cytometry analysis of T cells used CD3 (17A2) APC-eFluor 780, CD4 (GK1.5) APC, CD8a (53–6.7) eFluor 450 and Alexa Flour 488, CD44 (IM7) PerCP-Cyanine5.5, CD62L (L-selectin, MEL 14) FITC, CD49d (R1–2) PerCP-eFluor 710 or PE, Fc receptor blockers (anti-CD16/CD32 (clone 2.4G2)), mouse IgG (31205), and LIVE/DEAD™ Fixable Aqua Dead Cell Stain Kit for 405 nm excitation were purchased from eBioscience™/Thermo Fisher Scientific.

Methods

Cell lines

BRCA1-deficient BR5-*Akt* ovarian cancer cells were a kind gift from Dr. Sandra Orsulic (Cedars-Sinai).[24] CT26-Fluc-NEO colon cancer cells were purchased from Imanis Life Sciences, Rochester, MN, USA. BR5-Akt cells were lentivirus-transduced to constitutively express firefly2 luciferase. Cells were cultured in DMEM containing 10% FBS and 100 units/100 μg penicillin/streptomycin at 37°C and 5% CO_2.

Mouse models

Mice were purchased from Charles River or Jackson Laboratories. All animal protocols were approved by the Institutional Animal Care and Use Committee (IACUC) at the University of New Mexico (Albuquerque, NM, USA). To generate consistent engraftment and predictable disease progression, 2×10^5 BR5-*Akt*-Luc2 or CT26-FLuc cells in 200 μL PBS were administered by intraperitoneal (IP) injection in 6–8-week-old FVB (female) or BALB/c (female and male) mice.[25] For subcutaneous tumors, cells were administered by scruffing the loose skin on the dorsal side of the neck and injecting cells in 100 μl PBS. Intravenous administration was performed retro-orbitally. Mice were sacrificed when moribund or when they gained 10 g of weight with the presence of ascites. Mice were monitored and weighed every 2–3 days.

Cryo-silicification of cancer cells

BR5-*Akt* or CT26-luc cells were washed with PBS, followed by physiological saline (154 mM NaCl), and then suspended in silicic acid solution containing 10 mM TMOS, 100 mM NaCl and 1.0 mM HCl (pH 3.0), at 1.5×10^6 cells ml^{-1}. Following a 10-min incubation at room temperature, the cell suspension was transferred to −80°C for 24 h or longer.

Coating silicified cells with cationic polymer and TLR ligand

Silicified cells (15×10^6) were thawed and washed in PBS, and then made cationic by suspending the cells in 10 ml of 0.2 mg ml^{-1} 25k linear PEI for 10 min with rotation. After washing with PBS, the supernatant was removed and 50 μg CpG (final

volume approximately 100 µl PBS) was added and incubated for 10 min with gentle mixing every 2 min. Next, 25 µg of MPLA was added, and the solution was incubated for another 10 min with gentle mixing every 2 min. Unbound TLR agonist was removed by washing the cells in PBS. Vaccine was resuspended in 1000 µl PBS.

Vaccination and immune checkpoint inhibitor (ICI) treatment of mice

Tumor-bearing FVB or BALB/c mice were vaccinated (see study timelines) by intraperitoneal, subcutaneous, or intravenous (retro-orbital) injection with silicified BR5-Akt-Luc or CT26-Fluc cells modified with TLR agonists using 3×10^6 cells per mouse in 50–200 µl of PBS. Intraperitoneal ICI treatment began 4 h post vaccination and was repeated every 2–3 days as indicated using 100 µg in 100 µl PBS anti-CTLA-4 (9H10) or anti-PD-1 (RMPI-14) antibody from Bio X Cell, (Lebanon, NH, USA). Mice that cleared all tumor cells based on IVIS Spectrum bioluminescent imaging were re-challenged with 2×10^5 BR5-Akt-Luc2 cancer cells at a later date where indicated. All control mice received sham PBS injections (100–200 µl per mouse).

Omentectomy

Murine omentectomies were performed according to Institutional Animal Care and Use Committee (IACUC) standards on an approved protocol. Mice were anesthetized using 3–4% isoflurane in oxygen. Once anesthetized, mice were moved to a sterile warming bed in the supine position with a nose cone to continue anesthesia throughout the procedure. The surgical site was shaved to prevent contamination and excess fur. Mice were injected subcutaneously with Buprenorphine (0.1 mg/kg) near the incision site for analgesia for pain management. A 1.5–2 cm vertical incision was made through the skin and peritoneum directly below the sternum to expose the peritoneal cavity. The greater curvature of the stomach was identified, with the omentum attached. The greater omentum was removed above the pancreas and at the spleen. The peritoneum was closed using a running stitch with absorbable suture (vicryl or similar). The outer layer of skin was closed using wound-closing clips/staples. After surgery, mice were placed into a warming incubator for recovery. Animals were monitored for 30 min post-operative and then daily for signs of distress and/or morbidity for one week.

BR5-Akt-Luc2 cancer cells (2×10^5 in 200 µl PBS) were administered by intraperitoneal injection after removal of the surgical clips (7 days post-operative). Mice were vaccinated or injected intraperitoneally with PBS on Days 4 and 11 post tumor cell injection.

Antibody neutralization studies

All neutralization antibodies (BioXCell, Lebanon, NH, USA) were administered by intraperitoneal injection of 100 µg each in a total volume of 200 µl PBS. For T and B cell neutralization, mice were administered a combination of anti-CD4 (GK15) and anti-CD8a (53–6.7) T cell, or anti-B220 (RA3.3A1/6.1) and anti-CD19 (ID3) B cell antibodies every 3 days beginning one day prior to vaccination. For myeloid neutralization, mice were administered a combination of anti-CD11b (M1/70) and anti-PDCA-1 (927), or anti-Ly6G/Ly6C (Gr-1, clone RB6-8C5) antibody every 2 days. For vaccine biodistribution studies, mice were administered anti-CD11b antibody 24 h prior to intraperitoneal injection with CTFR vaccine.

Imaging tumor burden

For *in vivo* monitoring of tumor burden, mice were administered 150 mg luciferin/kg by intraperitoneal injection, with a 10-min delay before imaging. Mice were anesthetized using 2.5% isoflurane, and 2D/3D bioluminescence images were acquired using the IVIS® Spectrum In Vivo Imaging System (PerkinElmer, Waltham, MA, USA). ROI measurements of total flux (photons/sec) or fluorescence (for vaccine) were acquired using Living Image® 4.7.3 Software (Perkin Elmer).

Biodistribution of vaccine

To track vaccine cells *in vivo*, cancer cells were stained with CellTrace™ Far Red (CTFR) or carboxyfluorescein diacetate succinimidyl ester (CellTrace™ CSFE; ThermoFisher), and then silicified and functionalized with PEI, CpG, and MPLA. 3×10^6 fluorescent vaccine cells in 200 µl PBS were administered by intraperitoneal injection to FVB mice with disseminated cancer (19 days post BR5-Akt-Luc2 tumor challenge) or cancer-challenged mice post-vaccination. Twenty-four hours later, mice were euthanized in accordance with Institutional Animal Care and Use Committee (IACUC) at the University of New Mexico (Albuquerque, NM, USA), and peritoneal tissues were frozen in optimal cutting temperature (O.C.T.) compound. Sectioned tissues were fixed in ice-cold acetone for 15 min, blocked for non-specific binding, and incubated with anti-mouse CD11b (M1/70) and anti-mouse EPCAM (G8.8) antibody (1:50). Tissues were washed in PBS and slides were cover-slipped using Prolong Gold Mounting Media containing DAPI. Images were acquired using a 63X/1.4NA oil objective in sequential scanning mode using a Leica TCS SP8 confocal microscope. Tiled images are composites of 179 and 1022 images taken using a 20X or 63X objective, respectively and assembled using the Leica stitching algorithm with smooth blending.

To study *in vivo* tissue biodistribution, CTFR-labeled silicified vaccine cells were administered to FVB mice 18 days post tumor challenge. On Day 18–19, mice were imaged using the IVIS spectrum at 640/680 (excitation/emission). Organs were collected and imaged. Regions of interest were drawn on each organ to measure fluorescent intensities.

Immune cell phenotyping

Single-cell suspensions were first blocked with PBS containing 1% BSA. Next, samples were surface stained with conjugated primary antibodies (1:100 dilution) at 4°C for 30 min in the dark. Samples were then washed and analyzed immediately or stored in 4% paraformaldehyde at 4°C. Phenotyping was performed using the Attune NxT Flow Cytometer and analyzed using FlowJo (10.6) (Becton, Dickinson and Company).

Spectral flow cytometry

Ascites was collected from mice on Day 19 post cancer cell injection by making a midline cut and removing the skin covering the peritoneal cavity. A small incision was made to the parietal peritoneum and a pipet was inserted to remove ascites, following by injection of 2–4 ml of cold PBS with collection repeated. Cells were stained with fluorescent primary antibodies (1:100 dilution) for 30 min at 4°C, followed by a PBS wash and subsequent staining with Live/Dead stain for 5 min at room temperature. Cells were washed again in PBS and then fixed in 2% paraformaldehyde. Phenotyping was performed using the Cytek® Aurora Full Spectrum Flow Cytometer and analyzed using SpectroFlo® Flow Cytometry Software v3.0 (Cytex Biosciences, Fremont, CA, USA) and FlowJo (10.6) (Becton, Dickinson and Company; Franklin Lakes, NJ, USA). Relative numbers of CD45$^+$ cells were calculated based on the number of CD45$^+$ cells in 2×10^6 total events.

Blood metabolite measurements

Blood was collected by retro-orbital withdrawal using EDTA to prevent blood clotting. Blood metabolites were measured on Day 19 using the Vetscan VS2 Analyzer and Comprehensive Diagnostic Profile discs (Zoetis, Parsippany, NJ, USA) as described by the vendor.

Statistical Analysis

Measurements in this study were obtained from distinct samples. GraphPad Prism 10.0.3 (GraphPad Software; Boston, MA, USA) was used to perform statistical analysis. Kaplan-Meier survival curves were analyzed using Log-rank Mantel-Cox and Match SPSS and SAS tests for two and multiple group comparisons, respectively. For tumor burden comparisons, one-way or two-way ANOVAs with multiple t-test comparisons were performed, assuming all rows are sampled from populations with the same scatter. Where indicated, column statistics were analyzed using unpaired, two-tailed parametric t tests with equal standard deviation (SD). Graphs include means and SD error bars.

Results

Localization and cellular association of silicified vaccine cells following intraperitoneal injection

Fagarasan and colleagues[26] demonstrated that bacteria are internalized by macrophages within 3 h of peritoneal injection. Lipopolysaccharide (LPS), derived from gram-negative bacteria stimulates a rapid decline in the number of peritoneal macrophages in LPS-sensitive mice, a phenomenon coined the macrophage disappearance reaction (MDR).[17] We hypothesized that similar mechanisms would be engaged in response to silicified vaccine cells presenting pathogen associated molecular markers, including MPLA (a nontoxic derivative of the lipid A region of LPS[27]), leading to induction or restoration of anti-tumor immunity. To test this, we first monitored localization and cellular association of Cell Trace™ Far Red (CTFR)-labeled vaccine following peritoneal administration.

Silicified cancer cell vaccine was prepared as previously published.[2] Briefly, syngeneic cancer cells were biomineralized in an acidic silicic acid solution, followed by coating with 25k linear polyethyleneimine (PEI), CpG oligonucleotide 1826, and monophosphoryl lipid A (MPLA) (Figure 1a). We previously demonstrated that intraperitoneal, but not subcutaneous administration, consistently cleared early-stage BR5-*Akt*-Luc2 ovarian cancer.[2] Here we show the intravenous administration is also ineffective at clearing ovarian cancer (Figure S1).

Localization and cellular association of fluorescent-labeled vaccine cells were monitored longitudinally using flow cytometry and fluorescent imaging. Immediately after injection (30 min), vaccine cells were rapidly internalized by myeloid cells with subsequent enrichment in omental tissues. Specifically, silicified vaccine cells were observed to associate predominately with CD11b$^+$ myeloid cells (Figure 1b–c). CD11b$^+$ cells in mice with metastatic ovarian cancer include macrophages, monocytes, dendritic cells, and neutrophils/myeloid-derived suppressor cells (MDSC) (Figure S2). The proportion of ascites CD11b$^+$ cells compared to other peritoneal cells increased in response to vaccine injection, however, the percentage of CD11b$^+$ cells with internalized vaccine decreased rapidly (Figure 1c). Similar to the disappearance of bacteria, the disappearance of myeloid cells with internalized vaccine is due to MDR, whereby large peritoneal macrophages migrate to FALCs by a combination of macrophage released fibrin-induced aggregation and integrin-based adhesion.[28] Thus, vaccine cells presenting microbial molecules are rapidly internalized by peritoneal myeloid cells, with rapid migration of myeloid cells to lymphoid clusters. An example of a silicified vaccine cell internalized by an ascites myeloid cell is shown in Figure S3.

Representative independent and merged images of peritoneal tissues and ascites from a tumor-bearing mouse 1.5 h after intraperitoneal fluorescent vaccine injection are shown in Figure 1d. All mice were evaluated at 0.5, 1.5, 3.0, and 24 h after injection (Figure 1e). While silicified vaccine cells persisted in ascites fluid, they also accumulated in omental tissue during this time. We identified few silicified vaccine cells in mesenteric lymph nodes. Silicified vaccine cells were also enriched in tumor-burdened adipose tissues and superficial liver implants. These observations confirm that silicified cancer cells were retained in the peritoneal cavity and trafficked to sites associated with tumor implants within 3 h of vaccine administration.

Finally, bioluminescent and fluorescent images of tumor and vaccine cells at 24 h after vaccination are shown for a representative mouse in Figure 2a. 3D images of the intact mouse show corresponding robust cancer and vaccine signals originating from the omentum, which was confirmed on necropsy. The distribution of silicified vaccine cells from five mice is shown graphically (Figure 2b) along with fluorescent tissue images from each mouse (Figure 2c). Vaccine was largely located in adipose tissue with tumor implants, with smaller amounts found in the mesentery, ovary/uterus, and superficial liver implants. No fluorescent vaccine was detected outside of the peritoneal cavity during live animal imaging.
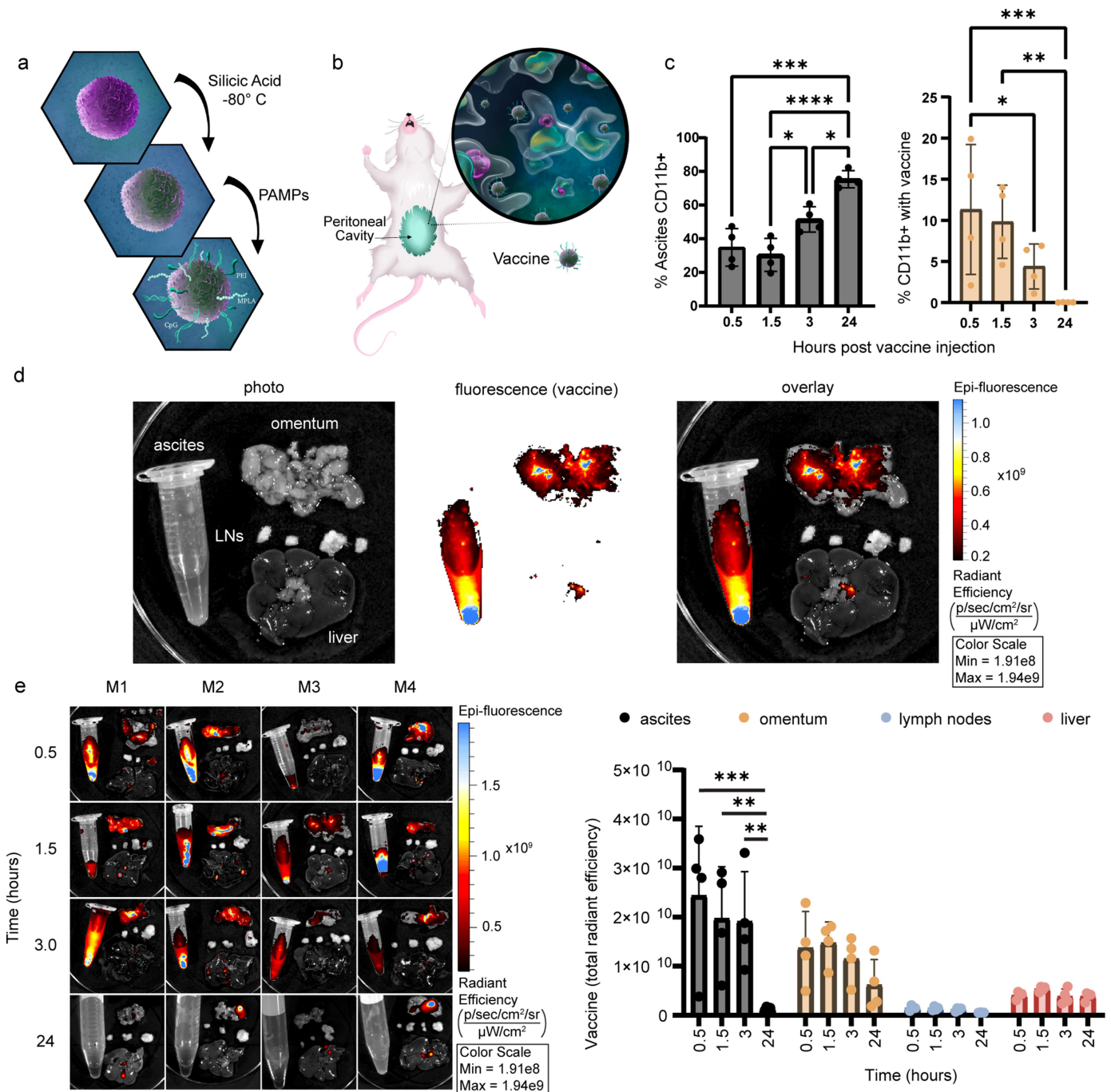
Figure 1. **Vaccine is rapidly internalized by ascites myeloid cells.** a) Artistic rendition depicting vaccine production from cancer cells (PAMPs: pathogen-associated molecular patterns). b) Artistic rendition showing phagocytosis of vaccine by peritoneal myeloid cells. c) Graph showing an increase in ascites CD11b $^+$ cells (left) and a decrease in ascites vaccine-laden CD11b$^+$ cells (right) as time progresses post intraperitoneal vaccine injection (n=4). d) Merged and independent photograph and fluorescent images of CellTrace™ Far Red (CTFR) stained vaccine in peritoneal tissues and ascites 19 days post BR5-*Akt*-Luc2 tumor challenge and 24 hours after intraperitoneal injection with 3 x 10^6 vaccine cells. e) Merged biodistribution images and graph showing CTFR vaccine fluorescence in ascites, omentum, and lymph nodes at various time points following intraperitoneal administration (n=4). Data is mean ± SD. Flow cytometry and biodistribution data were analyzed using a multiple comparisons test. *p<0.05, **p<0.01, ***p<0.001, ****p<0.0001.

Localization of vaccine in omental milky spots

To better define interactions of vaccine cells with FALCs at later time points, we specifically evaluated cellular association with milky spots (Figure 2d). Here we monitored localization and cellular association of CTFR-labeled vaccine 24 h after peritoneal injection in mice with disseminated ovarian cancer (Figure 2d). Snap frozen omental tissue was stained for the presence of CD11b$^+$ myeloid cells. Tumor implants were distinguished based on EpCAM expression. An entire omental section was imaged by tiling together 1022 fluorescent micrographs (Figure 2e). Distinct milky spots and tumor regions were observed, with vaccine localizing exclusively within the CD11b$^+$ immune cell clusters. Similar localization was seen in omentum from a unique tumor-bearing mouse (Figure 2f). Taken together, these
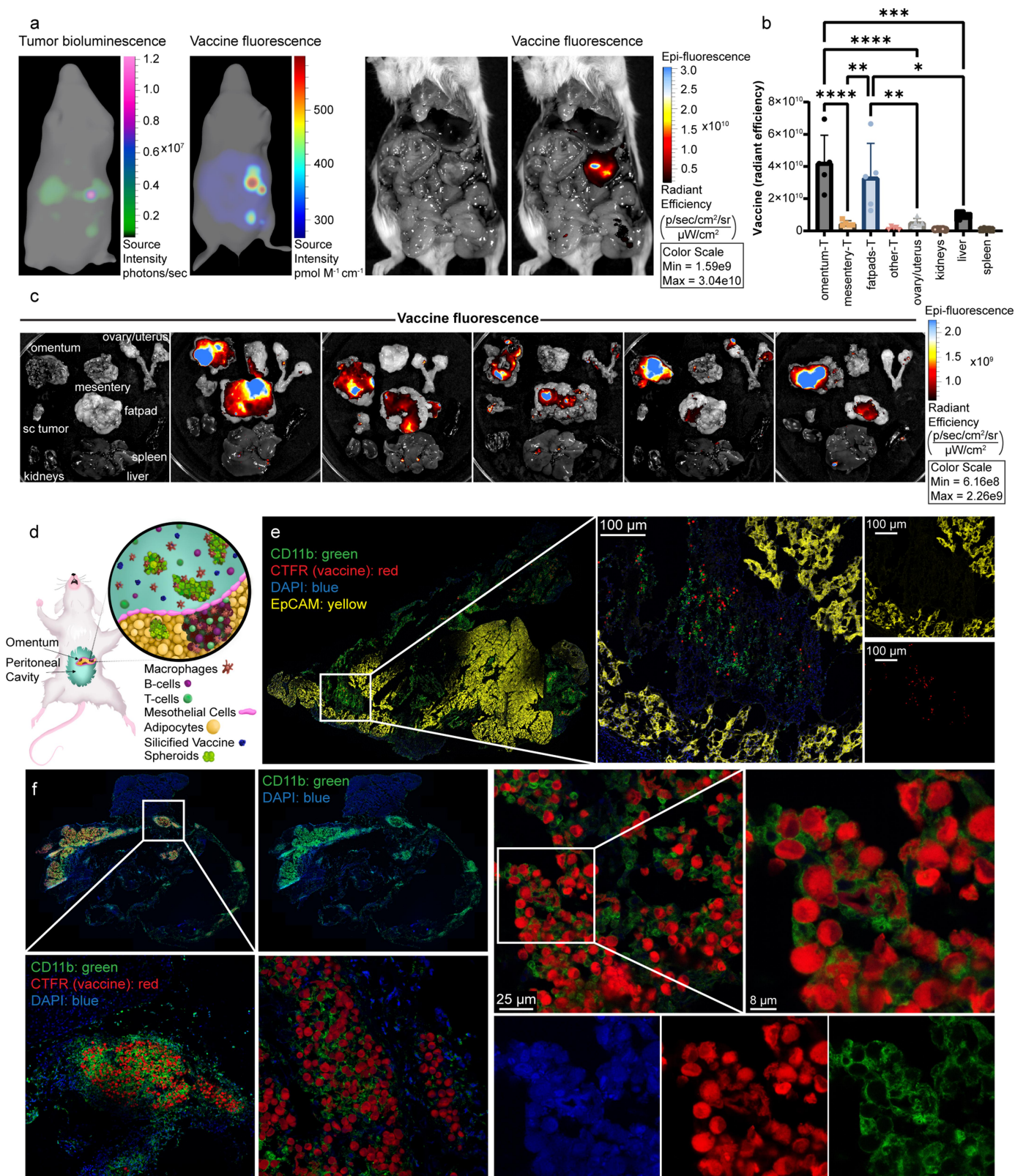
Figure 2. Vaccine selectively accumulates in fat-associated lymphoid clusters in tumor-burdened adipose tissues. Vaccine tissue biodistribution was determined 24 hours following intraperitoneal administration of 3 x 10^6^CTFR stained silicified vaccine cells in FVB mice 19 days post intraperitoneal injection with BR5-Akt-Luc2 ovarian cancer cells. a) 3D and 2D (open cavity) photographs with bioluminescent (cancer) or fluorescent (vaccine) overlays are presented from a representative mouse. b–c) Vaccine accumulation in peritoneal tissues is shown graphically (b) and as fluorescent overlays (c). d) Artistic rendition showing ascites cancer cells/spheroids and omental tissue with milky spots. e-f) Omental sections from representative mice were labeled with Alexa Fluor 488 anti-CD11b (M1/70) antibody, DAPI, and PE anti-EpCAM (G8.8). e) 1022 tiled, merged or independent fluorescent images (63X objective) showing vaccine, cancer and myeloid cells. f) 179 tiled fluorescent images (20x objective) of vaccine and myeloid cells, with boxed regions shown at higher magnification as independent or merged fluorescent images. Data is mean ± SD (n=5). Biodistribution data was analyzed by 1-way ANOVA (p<0.0001) and Tukey's multiple comparisons test (*p<0.05, **p<0.01, ***p<0.001, ****p<0.0001).

data indicate that TLR-labeled silicified vaccine cells co-opt mechanisms for pathogen clearance by peritoneal myeloid cells, resulting in their enrichment in FALCs.

Myeloid cell neutralization obstructs vaccine efficacy

Vaccine efficacy was evaluated in the presence of myeloid neutralization using either anti-mouse Gr-1 or anti-mouse CD11b/PDCA-1 (the latter expressed by plasmacytoid DC) antibodies in mice with ovarian cancer. Monotherapy with myeloid blockade had no impact on tumor growth (Figure 3a). However, myeloid blockade reduced vaccine efficacy, with loss of 90% of the treated mice due to excessive tumor burden. Ahn et al.[29] similarly demonstrated no impact of Gr-1 mAb or CD11b mAb (in the absence of radiation) monotherapy on tumor growth. Vaccine biodistribution and confocal microscopy studies showed continued phagocytosis and trafficking of vaccine to FALCs by CD11b^{+} myeloid cells following CD11b (Mac-1) epitope blockade (Figure 3b–c). In support of this, Tang et al.[30] reported that TLR ligands augment phagocytosis efficiency, alleviating the need for FcRs and CD11b.

Further highlighting the relevance of CD11b^{+} cells in the peritoneal cavity is the expression of CD11b on omental DCs that have the ability to cross present (CD11b^{+}/CD11c^{+}/MHCII^{hi}/Ly6C^{−}/CD103^{−}).[11] Also, Joshi et al.[31] reported that TIM4^{+} large peritoneal macrophages efficiently capture and cross-present tumor-associated antigens. Liu et al.[32] reported that CD154 and CD11b interactions are needed to increase

CD8^{+} T cell infiltration (into allografts). Ling et al.[33] showed that CD11b deficiency dampens DC-mediated TLR4-triggered responses in vivo contributing to impaired T cell activation. Therefore, CD11b epitope blockade likely reduces silicified cancer cell vaccine efficacy based on impaired T cell activation.

Vaccine remains efficacious in omentectomized mice

Preferential migration of both primary peritoneal cancer and metastatic cancer to the omentum, as well as the presence of milky spots, highlight the importance of the omentum in cancer progression and clearance.[34] To study the relevance of the omentum on vaccine efficacy, omentectomies were performed on mice prior to tumor cell injection and vaccination. Vaccination remained efficacious following omentectomy (Figure 4a). Vaccine biodistribution in control (PBS) mice showed high accumulation in tumor tissue originating from the surgical site (Figure 4b–e; Figure S4). While we anticipated that omentectomy would increase vaccine accumulation in mesentery FALCs, we found very little vaccine accumulation in the mesentery. Vaccine also partially localized in fat pads, but were not seen associated with myeloid cells in the selected tissue sections (Figure 4d).

Peritoneal B and T lymphocytes and macrophages are enriched following vaccination

Prior work characterized immune cells in untreated mice with ovarian cancer.[1] To explore the impact of intraperitoneal
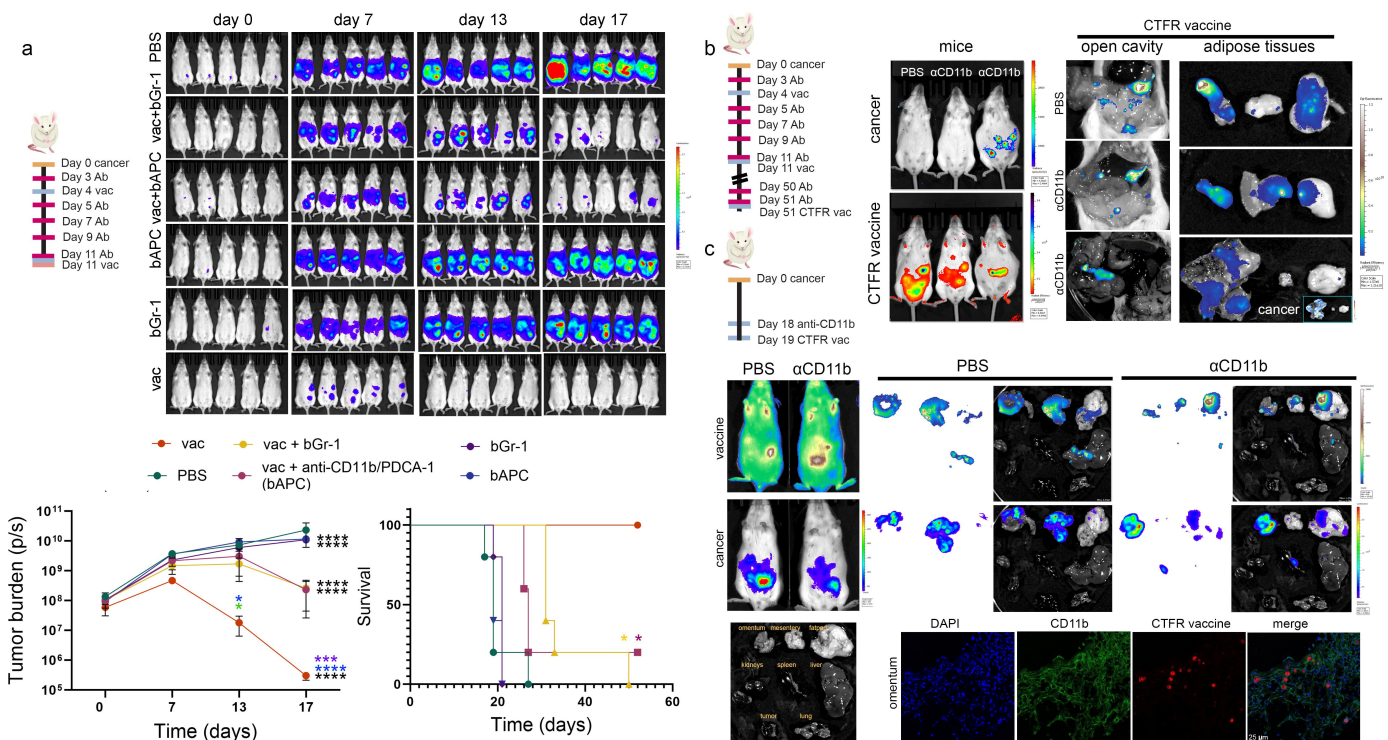

Figure 3. Myeloid cell neutralization ablates vaccine efficacy. Female FVB mice with BR5-Akt-Luc2 peritoneal metastases were administered one of the following every 48 hours: PBS, anti-Gr-1, or anti-CD11b/PNCA-1 by intraperitoneal injection (IP), and vaccine on Days 7 and 14. a) Timeline and IVIS bioluminescent images by group, with graphs of tumor burden and survival (n=5; *p<0.05, *** p< 0.001, ****p<0.0001, color indicates group being compared with). b) Two vaccinated mice and one receiving both vaccine and anti-CD11b/PDCA-1 (the latter burdened with cancer/ascites) were treated with PBS or anti-CD11b antibody at 18 and 4 hours prior to IP injection with CTFR vaccine. Twenty hours later, mice and excised adipose tissues were imaged for bioluminescence and fluorescence. c) FVB mice with ovarian cancer were IP injected with anti-CD11b antibody, followed 24 hours later by IP administration of CTFR vaccine. IVIS imaging of vaccine (fluorescence) and cancer (bioluminescence) in mice and excised organs. Confocal imaging of vaccine (red) and CD11b^{+} cells (green) in a representative omentum following CD11b neutralization.
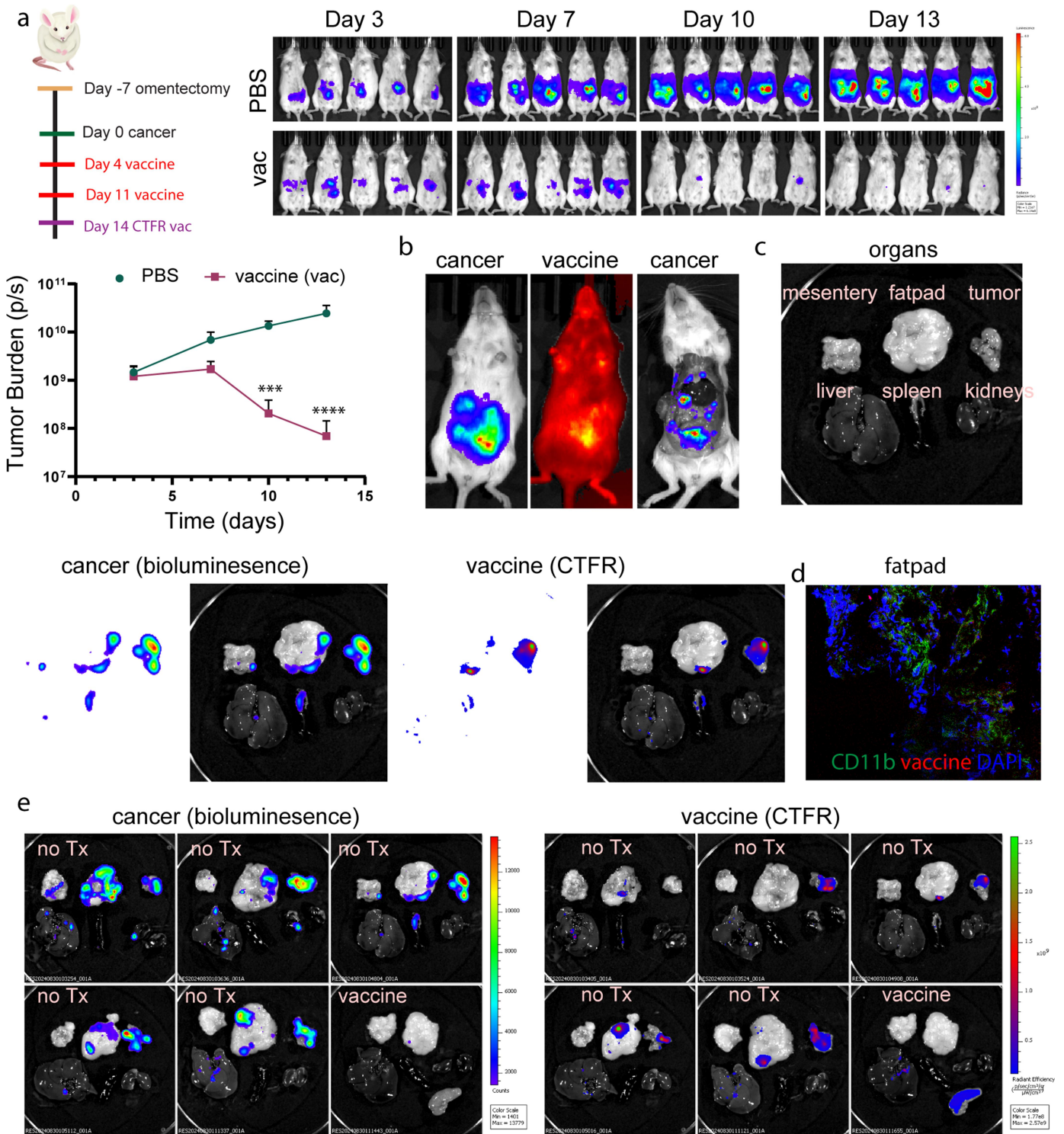
Figure 4. Vaccine efficacy persists following omentectomy. Omenta was surgically removed from female FVB mice. One-week later, mice were IP injected with BR5-Akt-Luc2 cells (day 0), followed by vaccine on Days 4 and 11. a) Timeline and longitudinal bioluminescent images, with graph of tumor burden by treatment group (***p<0.001, ****p<0.0001). b–e) On Day 14, 5 PBS (no Tx) mice and one vaccinated mouse were IP injected with CTFR vaccine and imaged for fluorescence and bioluminescence 24 hours later. b) Representative mouse images. c) Labeled organs from a representative mouse, with fluorescent and bioluminescent images of organs shown below. d) Confocal image showing CD11b+ cells (green) and sparse unassociated vaccine (red) in a fat pad section from a control (PBS) mouse. e) Bioluminescent and confocal images from 5 vaccinated untreated (PBS) mice and one vaccinated mouse. Cecum was included for the latter mouse based on high accumulation of vaccine.

vaccination and/or checkpoint inhibition on the tumor immune microenvironment, peritoneal cells collected post treatment (19 days post ovarian cancer implantation, and 2 or 5 days post final dose of CPI or vaccine) were characterized using spectral flow cytometry with TSNE plots shown in Figure 5. Vaccination increased the proportion of B cells, CD4+ T cells and macrophages, while treatment with anti-CTLA-4 antibody significantly increased the number of both macrophages and monocytes. Combination vaccination and anti-CTLA-4 antibody lead to the greatest increases in B cells, T cells, and myeloid cells.
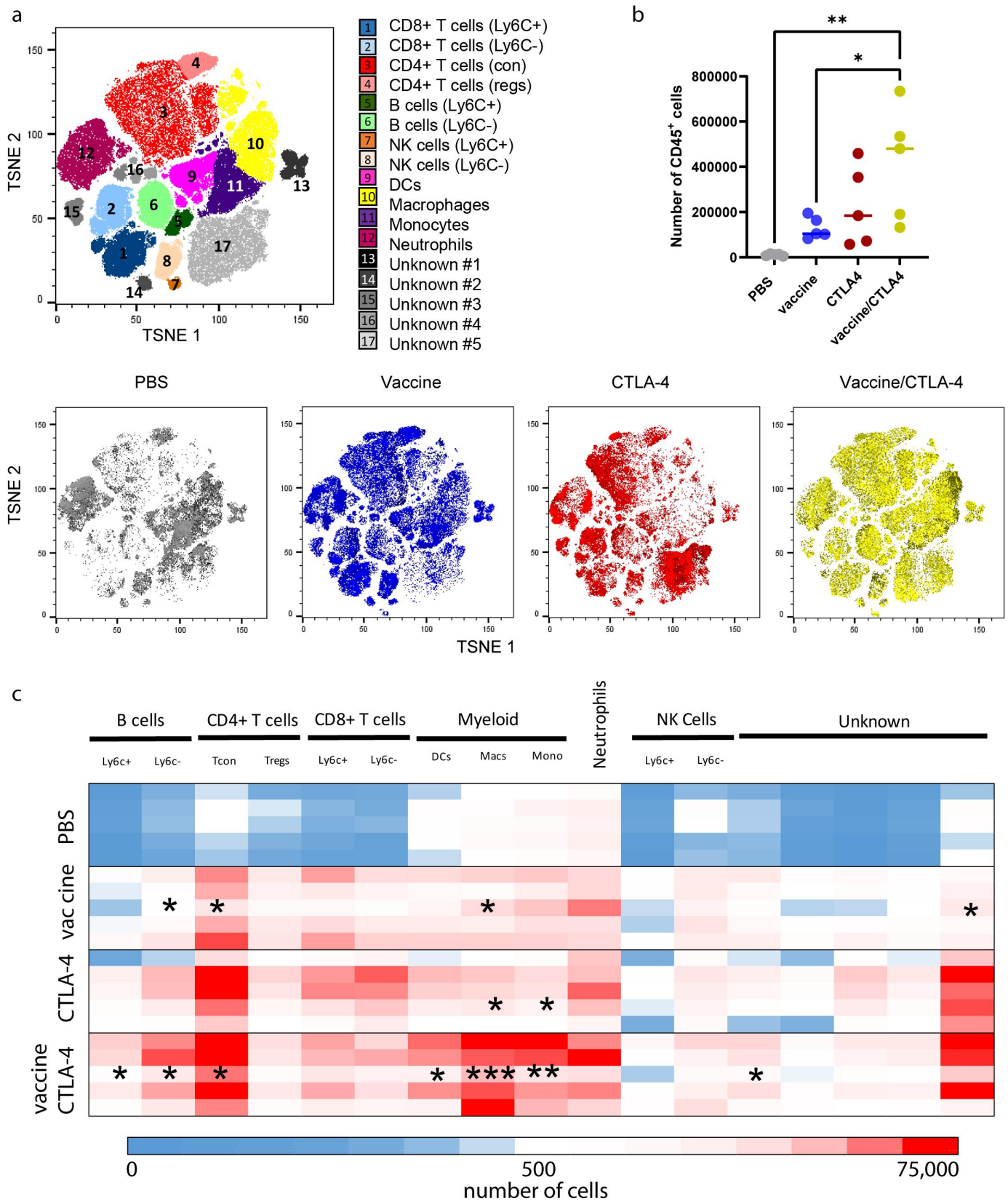
Figure 5. **Combination vaccine and anti-CTLA-1 expands myeloid, B cells and T cells, conditioning the landscape for anti-tumor responses.** Spectral flow cytometry was used to assess the cellular composition of ascites immune cells from FVB mice 19 days after BR5-Akt-Luc2 tumor cell injection. Mice (n=5) were administered PBS, vaccine, anti-CTLA-4, or both treatments by intraperitoneal injection on Days 7 and 14. a) TSNE plot showing cell populations, with TSNE plots of ascites cell populations by treatment group shown below. b) Relative number of CD45$^+$ cells in mice by treatment group (n=5, unpaired t test). c) Heat map showing immune cell composition for each group based on number of CD45$^+$ cells (* p<0.05, ** p< 0.01, *** p<0.001).

Elevated numbers of myeloid and T cells are supportive of antigen driven immune responses induced by vaccine, with augmented immune activation following combination therapy with immune checkpoint blockade. Combination therapy also lead to the greatest increase in relative number of CD45^{+} cells (Figure 5b).

Vaccine efficacy is dependent on T cells but not B cells

B cells contribute to antitumor immunity by antigen presentation, cytokine production, and production of soluble antigen specific antibodies. In ovarian cancer, B cell IgA production has been shown to promote myeloid cell-dependent killing of cancer cells.[35] To define a role for B cells in generating vaccine-mediated immune therapy, we evaluated treatment efficacy following B cell depletion using neutralizing antibodies. We found that B cell depletion did not alter

vaccine efficacy (Figure 6a–c). We previously demonstrated that adoptive transfer of peritoneal CD8-enriched T cells from vaccinated to naïve mice blocked tumor growth upon re-challenge with cancer cells.[2] Here, T cell depletion using CD4 and CD8 specific antibodies rendered the vaccine non-functional. We interpret these results as confirmation that vaccination induces T cell-mediated immunity that is essential for reducing tumor burden. In support of this, in a separate cohort of mice, Day 25 peritoneal effector memory CD4^{+} and CD8^{+} T cells were elevated following vaccination, with both populations expressing CD49d, a cell surface β1-integrin that identifies antigen-specific T cells (Figure 6d).[36–38] Elevated beta integrins facilitate effector T cell surveillance functions, enabling T cells to enter tissues at sites of inflammation.[39] Splenic effector memory T cell populations were not altered following peritoneal vaccination, supporting regional localization of memory cells.
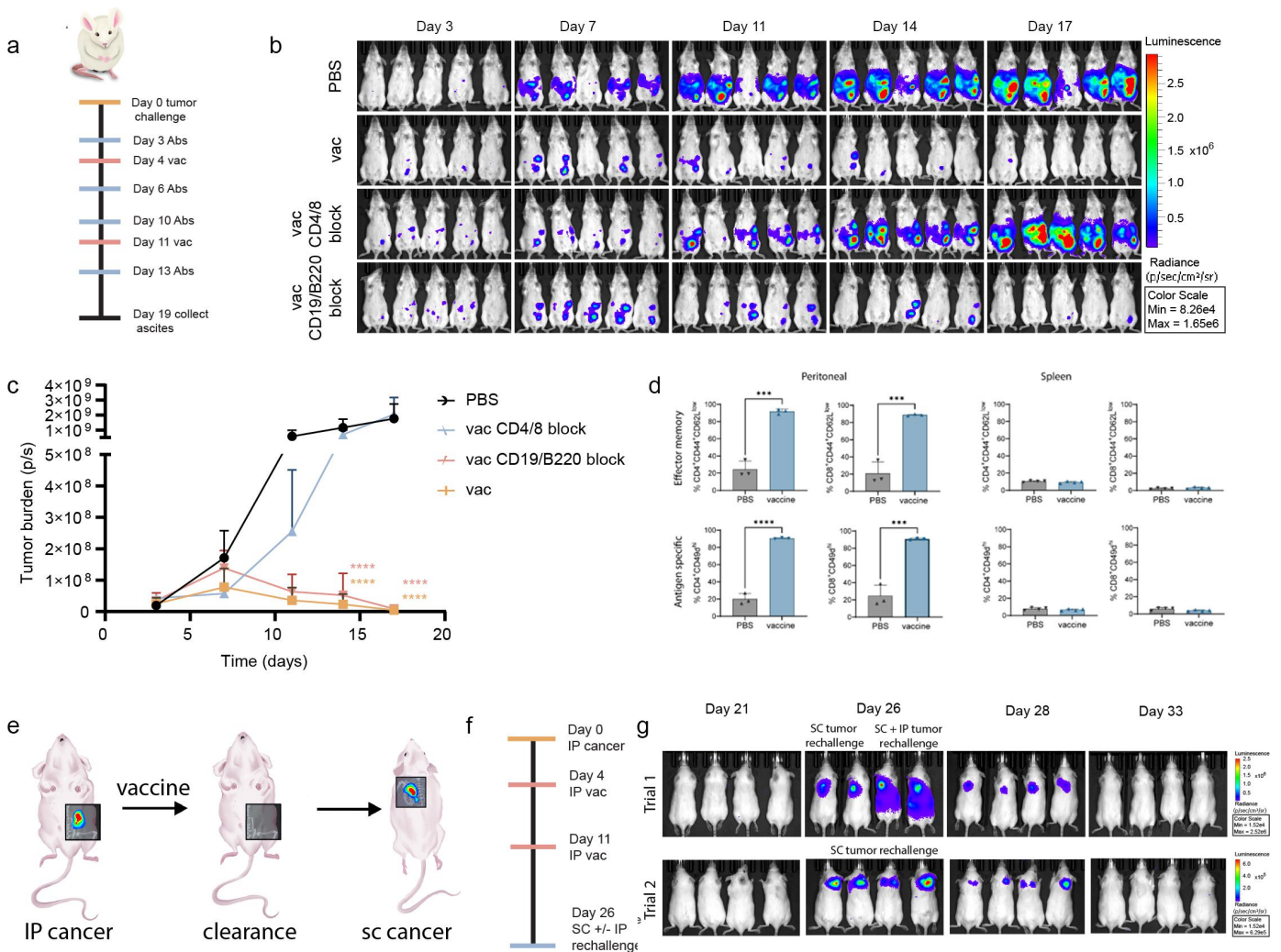

Figure 6. **Vaccine efficacy is T cell dependent, leading to systemic immunity.** FVB mice with BR5-Akt-Luc2 cancer were administered 2 doses of silicified cancer vaccine (Days 4 and 11), with or without pretreatment plus concurrent treatment with neutralizing antibodies against CD19/B220 or CD4/CD8, the later given twice weekly via intraperitoneal injection. a) Timeline. b) Longitudinal IVIS bioluminescent images. c) Tumor burden graph (n=5; data are mean ± SD. Tumor burden data was analyzed by 2-way ANOVA (P<0.05) and Tukey's multiple comparisons test. ****p<0.0001). d) Flow cytometry was used to define changes in peritoneal and splenic T cell type following intraperitoneal vaccination of mice with BR5- Akt-Luc2 ovarian cancer. Peritoneal fluid/wash was collected for analysis on Day 25 (n=3; unpaired, two-tailed, parametric t-test and SD error bars). The percent of peritoneal or splenic CD4+ and CD8+ T-cells with effector memory (CD44+CD62Llow) or antigen specific (CD49dhi) phenotypes are shown. e–g) Schematic (e), timeline (f), and IVIS bioluminescent images (g) of tumor cleared FVB mice rechallenged by subcutaneous, with and without intraperitoneal, injection with BR5-Akt-Luc2 cancer cells 26 days post initial intraperitoneal BR5-Akt-Luc2 cancer injection and following 2 doses of vaccine administered by intraperitoneal injection on Days 4 and 11 (n=8).
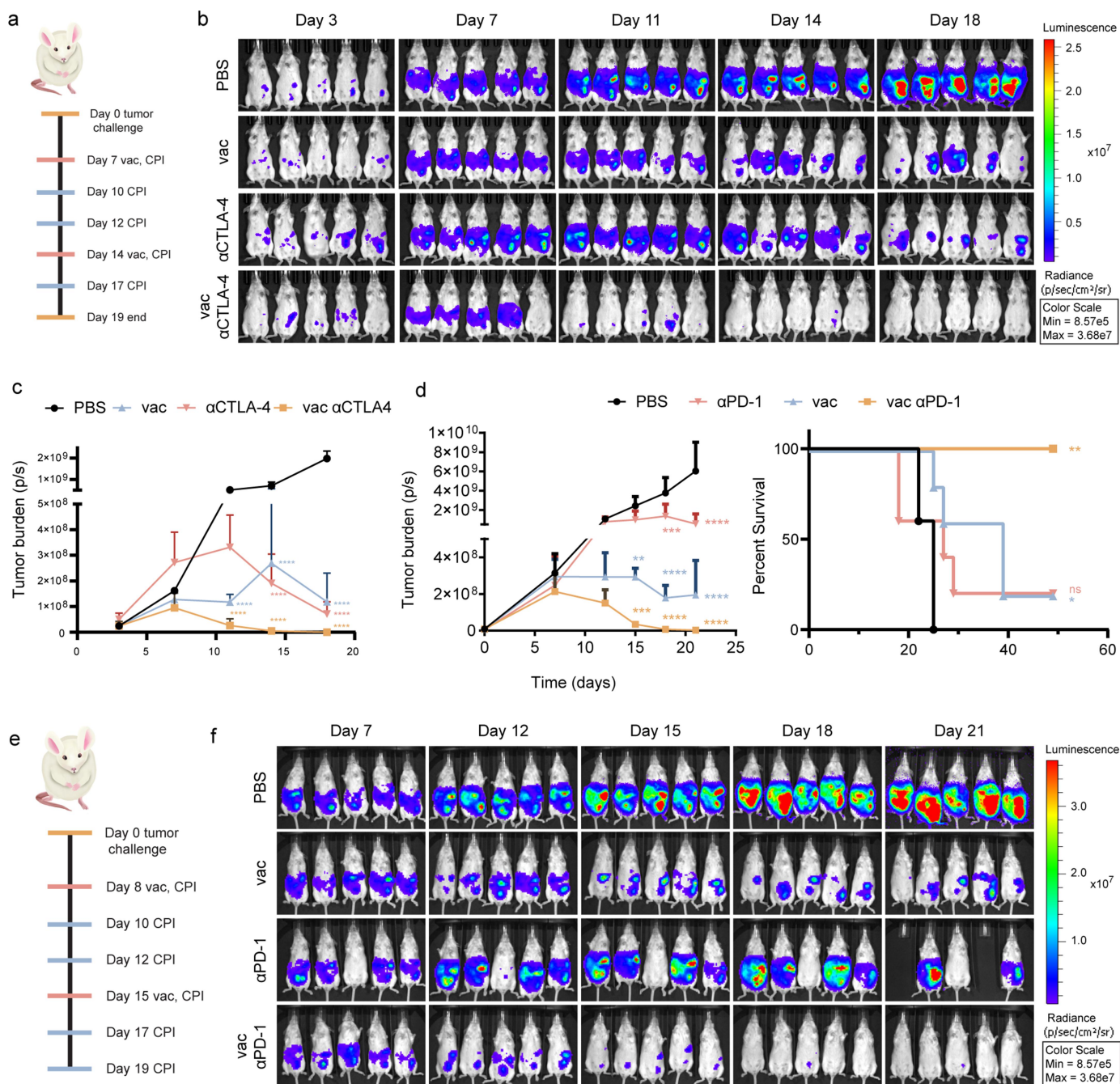
Figure 7. Combination vaccine and checkpoint inhibition therapy eradicates ovarian cancer. a–c) FVB mice with advanced BR5-Akt-Luc2 cancer were administered 2 doses of vaccine on Days 7 and 14, and/or anti-CTLA-4 antibody every 2-3 days via intraperitoneal injection. a) Timeline. b) IVIS bioluminescent images. c) Longitudinal tumor burden graph. d–f) FVB mice with advanced BR5-Akt-Luc2 were administered 2 doses of vaccine on Days 8 and 15, and/or anti-PD1 antibody every 2-3 days via intraperitoneal injection. d) Graphs showing longitudinal tumor burden and survival. e) Timeline. f) IVIS bioluminescent images. Data is mean ± SD (n=5). Tumor burden data was analyzed by 2-way ANOVA (P<0.05) and Tukey's multiple comparisons test. The survival curve was analyzed using a Log-rank (Mantel-Cox) comparison of curves. Data is mean ± SD (n=5). *p<0.05, **p<0.01, ***p<0.001, ****p<0.0001.

Intraperitoneal vaccination induces protective systemic immunity

To deterimine if intraperitoneal vaccination could induces systemic immune memory, we performed secondary tumor challenges in treated mice at extraperitoneal sites. All mice received subcutaneous tumor cell injections, with two mice also receiving intraperitoneal vaccine to evaluate if activation of regional peritoneal immune cells is needed for systemic immunity. Cancer failed to engraft in all mice (Figure 6e–g),

supporting the existence of both resident and systemic immune memory.

Immune checkpoint blockade enhances vaccine efficacy in ovarian cancer mouse models with delayed treatment

Immune checkpoint inhibitor (ICI) monotherapy has thus far shown limited efficacy in clinical trials for patients with ovarian cancer.[40,41] Using MEXPRESS, Gai and colleagues[42] discovered that CTLA-4 is strongly expressed in residual high-grade serous

ovarian carcinoma tumors, with a significant influence on overall survival. We previously demonstrated that DC retain T cell stimulatory capacity in late disease and expected ICI therapy to restore impeded T cell responses.[19] Here, preclinical outcomes of combination anti-CTLA-4 antibody and vaccination were evaluated. Mice bearing BR5-*Akt*-luc2 tumors with treatment beginning on Day 7 with anti-CTLA-4 antibody or vaccine monotherapy displayed similar reductions in tumor burden (Figure 7a–c). Combination anti-CTLA-4 antibody and vaccine was able to clear all detectable tumors, but was not significantly better than vaccine monotherapy. All treatments reduced tumor burden significantly more than controls ($p < 0.0001$).

Treatment with immune checkpoint inhibitor anti-PD-1 antibody was also studied to mitigate the impact of upregulation in the tumor microenvironment. Both vaccine monotherapy and anti-PD1 antibody monotherapy beginning on Day 8 reduced tumor burden but were unable to eliminate

all cancer (Figure 7d–f). Combination vaccine and anti-PD-1 antibody successfully eliminated all detectable cancer in five of five mice treated mice, with improved survival of all mice ($p < 0.01$). In summary, vaccine synergized with PD-1 immune checkpoint blockade.

Immune-related adverse events (irAEs) are reported to occur in 90% of patients treated with anti-CTLA-4 and 70% of patients treated with anti-PD-1/PD-L1.[43,44] To evaluate irAEs in treated mice, serum metabolites were measured 12 days after ICI and vaccine initiation. Alkaline phosphatase (ALP), a marker that may be elevated in the setting of liver damage, was elevated in mice treated with anti-CTLA-4 monotherapy ($p = 0.04$). No markers of toxicity were seen in mice receiving combination anti-CTLA-4 and vaccine, (Figure S5). No significant differences existed between monotherapy and combination treatment groups for alanine aminotransferase (ALT), blood urea nitrogen (BUN), and total bilirubin. In
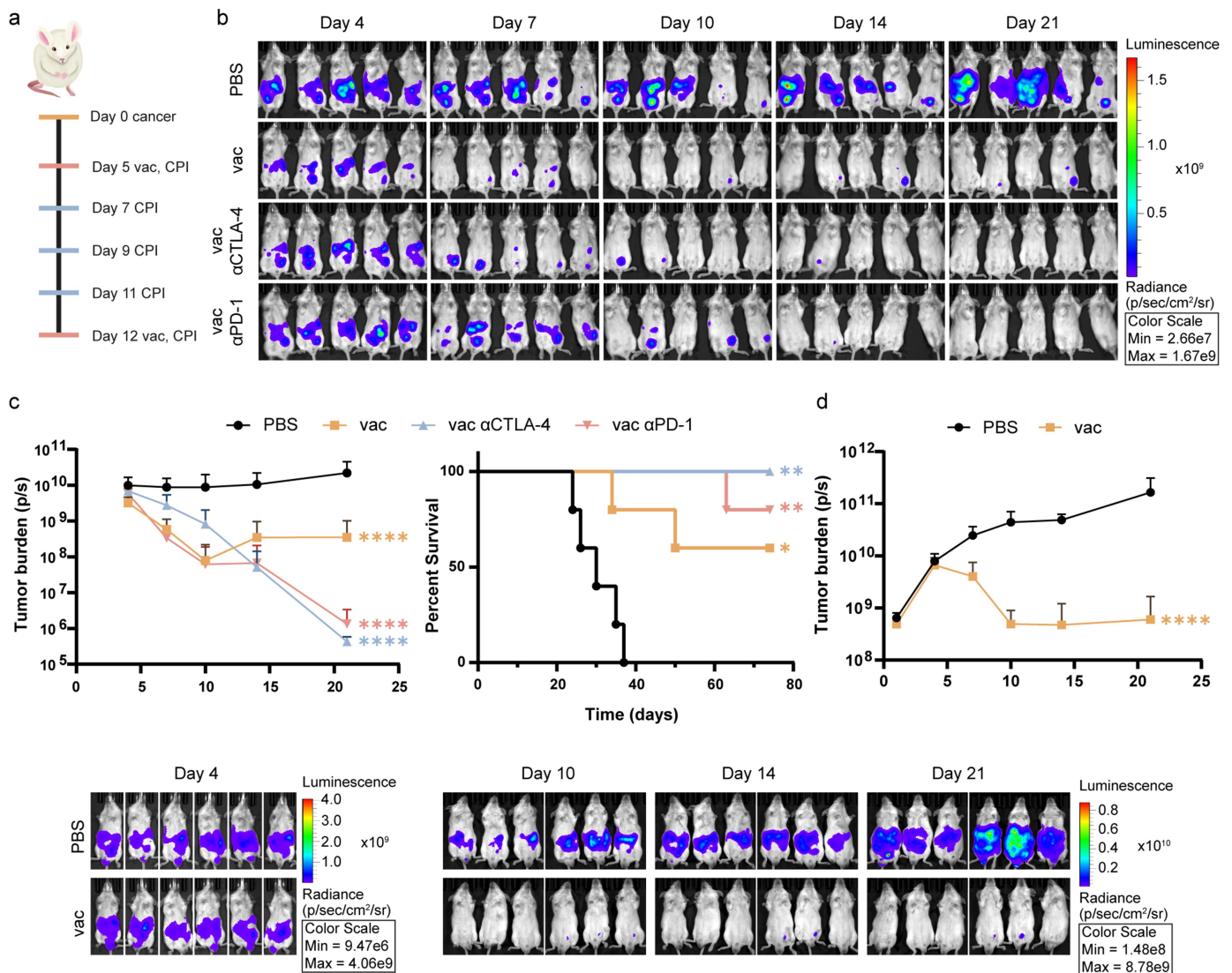

Figure 8. Vaccine ablates cancer in a mouse model of colon cancer. a) Timeline. b) Longitudinal IVIS bioluminescent images of female BALB/c mice with peritoneal CT26-Fluc colon cancer shown by treatment group with intraperitoneal vaccination beginning on Day 5, and intraperitoneal anti-CTLA-4 or anti-PD-1 given every 2-3 days. c) Tumor burden and survival curves. d) Graph and IVIS images showing longitudinal tumor burden in male BALB/c mice with CT26-Fluc colon cancer (same timeline). Data is mean ± SD (n=5); p-values (compared to PBS group) were calculated using a two-way ANOVA with Tukey's multiple comparisons test for tumor burden and the Mantel-Cox test for survival curves. *p <0.05, **p <0.01, ***p<0.001, ****p = <0.0001.

summary, no evidence of irAEs were present in mice treated with combination vaccine and immune checkpoint inhibitor based on serum metabolites.

Vaccine efficacy in a mouse model of colon cancer metastasis

Colorectal cancer is also associated with the development of peritoneal carcinomatosis.[45,46] The CT26 mouse model is highly undifferentiated and proliferative, and is used as a microsatellite stable (MSS) mismatch repair proficient (MMRp) model.[47] Metastatic colon cancer was established in female BALB/c mice by intraperitoneal injection of CT26-Fluc cells. Intraperitoneal treatment of mice with vaccine monotherapy reduced tumor burden in all mice ($p < 0.0001$ compared to control) and led to long term survival in three of five mice ($p < 0.05$, Figure 8a–c). Combination vaccine and immune checkpoint inhibitor therapy demonstrated that either anti-PD-1 or anti-CTLA-4 together with vaccine reduce tumor to undetectable levels. All mice treated with vaccine and anti-CTLA-4 survived to the study endpoint of 74 days, despite the CT26 cell line being considered microsatellite stable.[48] Vaccine monotherapy was similarly effective in male BALB/c mice with colon cancer ($p < 00001$, Figure 8d). In summary, silicified tumor cell vaccination is effective in disseminated solid tumor models, and can enhance response to ICI in late stages of disease.

Discussion

We previously demonstrated that vaccination with TLR agonist presenting silicified tumor cells activates innate immune pathways resulting in effective anti-tumor T cell immunity and therapeutic benefit in syngeneic high-grade serous ovarian cancer models.[2,49,50] Here we demonstrate the critical role of local immune networks in achieving optimal disease control. Importantly, we also confirm that intraperitoneal administration successfully induces systemic immunity, presenting a strategy to overcome hurdles to vaccine therapy in ovarian cancer. Evidence that the silicified cancer cell vaccines are highly effective in disseminated colorectal cancer further expands the impact of these findings.

Labeling silicified tumor cells with pathogen-associated molecules was shown to co-opt innate immune mechanisms in the peritoneal cavity to rapidly transport vaccine cells to FALCs. Colocalization of lymphoid clusters and cancer in adipose tissues facilites the development of anti-tumor immunity at the tumor site. Here we presented the essential role of myeloid cells in trafficking vaccine to milky spots. We also demonstrated the presence of CD4^{+} and CD8^{+} effector memory T cells expressing the antigen-specific marker CD49d in the peritoneal cavity, but not in the spleen of mice bearing ovarian cancer following vaccination. In keeping with evidence that specific T cell immunity generated in the peritoneal cavity provides systemic protection from colon and ovarian cancer in mice,[2,51] therapeutic vaccination with silicified cancer cells was protective against secondary local and systemic cancer challenge.

This study demonstrates that directly targeting tumor-associated immune networks can substantially enhance the therapeutic efficacy of vaccination in models with low tumor burden, presenting a rationale for vaccination as consolidation therapy after frontline treatment. As cancer progresses and adaptive immune suppression increases in the tumor micro-environment, vaccination efficacy benefits from addition of immune checkpoint inhibitors, providing a strategy that could be adapted for recurrent ovarian cancer.

Disclosure statement

No potential conflict of interest was reported by the author(s). RES and SA are inventors of patents and patent applications based on technology presented in this manuscript.

Authors contributions

RES designed the overall study. RES, and EB contributed to experimental design. RES, EB, BM, JA, LM, and EL conducted research and analyzed data. RES, EB, and SA wrote/edited the manuscript. All authors reviewed and approved the manuscript.

Availability of data and material

All figures have associated raw data. Graphpad prism tumor burden and survival files are available as source data.

Consent for publication

All authors have read the manuscript and approve it for submission.

Ethics approval

Murine omentectomies were performed according to Institutional Animal Care and Use Committee (IACUC) standards on an approved protocol.

References

1. Taylor EN, Wilson CM, Franco S, De May H, Medina LY, Yang Y, Flores EB, Bartee E, Selwyn RG, Serda RE. et al. Monitoring therapeutic responses to silicified cancer cell immunotherapy using PET/MRI in a mouse Model of disseminated ovarian cancer. Int J Mol Sci. 2022;23(18):10525. doi:10.3390/ijms231810525.
2. Guo J, De May H, Franco S, Noureddine A, Tang L, Brinker CJ, Kusewitt DF, Adams SF, Serda RE. Cancer vaccines from

cryogenically silicified tumour cells functionalized with pathogen-associated molecular patterns. Nat Biomed Eng. 2022;6(1):19–31. doi:10.1038/s41551-021-00795-w.

3. Meraz IM, Hearnden CH, Liu X, Yang M, Williams L, Savage DJ, Gu J, Rhudy JR, Yokoi K, Lavelle EC. et al. Multivalent presentation of MPL by porous silicon microparticles favors T helper 1 polarization enhancing the anti-tumor efficacy of doxorubicin nanoliposomes. PLOS ONE. 2014;9(4):e94703. doi:10.1371/journal.pone.0094703.

4. Savage DJ, Liu X, Curley SA, Ferrari M, Serda RE. Porous silicon advances in drug delivery and immunotherapy. Curr Opin Pharmacol. 2013;13(5):834–841. doi:10.1016/j.coph.2013.06.006.

5. Adams SF, Grimm AJ, Chiang CL, Mookerjee A, Flies D, Jean S, McCann GA, Michaux J, Pak H, Huber F. et al. Rapid tumor vaccine using Toll-like receptor-activated ovarian cancer ascites monocytes. J Immunother Cancer. 2020;8(2):e000875. doi:10.1136/jitc-2020-000875.

6. Koppe MJ, Boerman OC, Oyen WJ, Bleichrodt RP. Peritoneal carcinomatosis of colorectal origin: incidence and current treatment strategies. Ann Surg. 2006;243(2):212–222. doi:10.1097/01.sla.0000197702.46394.16.

7. Thomakos N, Diakosavvas M, Machairiotis N, Fasoulakis Z, Zarogoulidis P, Rodolakis A. Rare distant metastatic disease of ovarian and Peritoneal Carcinomatosis: a review of the literature. Cancers (Basel). 2019;11(8):1044. doi:10.3390/cancers11081044.

8. Foster JM, Zhang C, Rehman S, Sharma P, Alexander HR. The contemporary management of peritoneal metastasis: a journey from the cold past of treatment futility to a warm present and a bright future. CA Cancer J Clin. 2023;73(1):49–71. doi:10.3322/caac.21749.

9. Ardavin C, Alvarez-Ladron N, Ferriz M, Gutierrez-Gonzalez A, Vega-Perez A. Mouse tissue-resident peritoneal macrophages in homeostasis, repair, infection, and tumor metastasis. Adv Sci (Weinh). 2023;10(11):e2206617. doi:10.1002/advs.202206617.

10. Williams R, White H. The greater omentum: its applicability to cancer surgery and cancer therapy. Curr Probl Surg. 1986;23 (11):789–865. doi:10.1016/0011-3840(86)90007-9.

11. Carlow DA, Gold MR, Ziltener HJ. Lymphocytes in the peritoneum home to the omentum and are activated by resident dendritic cells. J Immunol. 2009;183(2):1155–1165. doi:10.4049/jimmunol.0900409.

12. Mebius RE. Lymphoid organs for peritoneal cavity immune response: milky spots. Immunity. 2009;30(5):670–672. doi:10.1016/j.immuni.2009.04.005.

13. Krist LF, Eestermans IL, Steenbergen JJ, Hoefsmit EC, Cuesta MA, Meyer S, Beelen RHJ. Cellular composition of milky spots in the human greater omentum: an immunochemical and ultrastructural study. Anat Rec. 1995;241(2):163–174. doi:10.1002/ar.1092410204.

14. Shimotsuma M, Takahashi T, Kawata M, Dux K. Cellular subsets of the milky spots in the human greater omentum. Cell Tissue Res. 1991;264(3):599–601. doi:10.1007/BF00319049.

15. Liu M, Silva-Sanchez A, Randall TD, Meza-Perez S. Specialized immune responses in the peritoneal cavity and omentum. J Leukoc Biol. 2021;109(4):717–729. doi:10.1002/JLB.5MIR0720-271RR.

16. Meza-Perez S, Randall TD. Immunological functions of the omentum. Trends Immunol. 2017;38(7):526–536. doi:10.1016/j.it.2017.03.002.

17. Barth MW, Hendrzak JA, Melnicoff MJ, Morahan PS. Review of the macrophage disappearance reaction. J Leukoc Biol. 1995;57 (3):361–367. doi:10.1002/jlb.57.3.361.

18. Perez-Shibayama C, Gil-Cruz C, Cheng HW, Onder L, Printz A, Morbe U, Novkovic M, Li C, Lopez-Macias C, Buechler MB. et al. Fibroblastic reticular cells initiate immune responses in visceral adipose tissues and secure peritoneal immunity. Sci Immunol. 2018;3(26). doi:10.1126/sciimmunol.aar4539.

19. Flies DB, Higuchi T, Harris JC, Jha V, Gimotty PA, Adams SF. Immune checkpoint blockade reveals the stimulatory capacity of tumor-associated CD103(+) dendritic cells in late-stage ovarian cancer. Oncoimmunology. 2016;5(8):e1185583. doi:10.1080/2162402X.2016.1185583.

20. Duraiswamy J, Turrini R, Minasyan A, Barras D, Crespo I, Grimm AJ, Casado J, Genolet R, Benedetti F, Wicky A. et al. Myeloid antigen-presenting cell niches sustain antitumor T cells and license PD-1 blockade via CD28 costimulation. Cancer Cell. 2021;39 (12):1623–42 e20. doi:10.1016/j.ccell.2021.10.008.

21. Chaurio RA, Anadon CM, Lee Costich T, Payne KK, Biswas S, Harro CM, Moran C, Ortiz AC, Cortina C, Rigolizzo KE. et al. Tgf-β-mediated silencing of genomic organizer SATB1 promotes tfh cell differentiation and formation of intra-tumoral tertiary lymphoid structures. Immunity. 2022;55(1):115–28 e9. doi:10.1016/j.immuni.2021.12.007.

22. Li R, Berglund A, Zemp L, Dhillon J, Putney R, Kim Y, Jain RK, Grass GD, Conejo-Garcia J, Mulé JJ. et al. The 12-CK score: global measurement of tertiary lymphoid structures. Front Immunol. 2021;12:694079. doi:10.3389/fimmu.2021.694079.

23. Zhang K, Xie X, Zou LH, Guo SQ. Tertiary lymphoid structures are associated with a favorable prognosis in high-grade serous ovarian cancer patients. Reprod Sci. 2023;30(8):2468–2480. doi:10.1007/s43032-023-01188-x.

24. Xing D, Orsulic S. A mouse model for the molecular characterization of brca1-associated ovarian carcinoma. Cancer Res. 2006;66 (18):8949–8953. doi:10.1158/0008-5472.CAN-06-1495.

25. Higuchi T, Flies DB, Marjon NA, Mantia-Smaldone G, Ronner L, Gimotty PA, Adams SF. CTLA-4 blockade synergizes therapeutically with PARP inhibition in BRCA1-deficient ovarian cancer. Cancer Immunol Res. 2015;3(11):1257–1268. doi:10.1158/2326-6066.CIR-15-0044.

26. Ha SA, Tsuji M, Suzuki K, Meek B, Yasuda N, Kaisho T, Fagarasan S. Regulation of B1 cell migration by signals through Toll-like receptors. J Exp Med. 2006;203(11):2541–2550. doi:10.1084/jem.20061041.

27. Salkowski CA, Detore GR, Vogel SN. Lipopolysaccharide and monophosphoryl lipid a differentially regulate interleukin-12, gamma interferon, and interleukin-10 mRNA production in murine macrophages. Infect Immun. 1997;65(8):3239–3247. doi:10.1128/iai.65.8.3239-3247.1997.

28. Zhang N, Czepielewski RS, Jarjour NN, Erlich EC, Esaulova E, Saunders BT, Grover SP, Cleuren AC, Broze GJ, Edelson BT. et al. Expression of factor V by resident macrophages boosts host defense in the peritoneal cavity. J Exp Med. 2019;216(6):1291–1300. doi:10.1084/jem.20182024.

29. Ahn GO, Tseng D, Liao CH, Dorie MJ, Czechowicz A, Brown JM. Inhibition of Mac-1 (CD11b/CD18) enhances tumor response to radiation by reducing myeloid cell recruitment. Proc Natl Acad Sci U S A. 2010;107(18):8363–8368. doi:10.1073/pnas.0911378107.

30. Tang Z, Davidson D, Li R, Zhong MC, Qian J, Chen J, Veillette A. Inflammatory macrophages exploit unconventional pro-phagocytic integrins for phagocytosis and anti-tumor immunity. Cell Rep. 2021;37(11):110111. doi:10.1016/j.celrep.2021.110111.

31. Joshi S, Lopez L, Morosi LG, Amadio R, Pachauri M, Bestagno M, Ogar IP, Giacca M, Piperno GM, Vorselen D. et al. Tim4 enables large peritoneal macrophages to cross-present tumor antigens at early stages of tumorigenesis. Cell Rep. 2024;43(4):114096. doi:10.1016/j.celrep.2024.114096.

32. Liu D, Ford ML. CD11b is a novel alternate receptor for CD154 during alloimmunity. Am J Transpl. 2020;20(8):2216–2225. doi:10.1111/ajt.15835.

33. Ling GS, Bennett J, Woollard KJ, Szajna M, Fossati-Jimack L, Taylor PR, Scott D, Franzoso G, Cook HT, Botto M. et al. Integrin CD11b positively regulates TLR4-induced signalling pathways in dendritic cells but not in macrophages. Nat Commun. 2014;5(1):3039. doi:10.1038/ncomms4039.

34. Feuer G, Briskin C, Lakhi N. Robotic omentectomy in gynecologic oncology: surgical anatomy, indications, and a technical approach. J Robot Surg. 2023;17(4):1381–1391. doi:10.1007/s11701-022-01519-1.

35. Biswas S, Mandal G, Payne KK, Anadon CM, Gatenbee CD, Chaurio RA, Costich TL, Moran C, Harro CM, Rigolizzo KE. et al. IgA transcytosis and antigen recognition govern ovarian cancer

immunity. Nature. 2021;591(7850):464–470. doi:10.1038/s41586-020-03144-0.

36. McDermott DS, Varga SM. Quantifying antigen-specific CD4 T cells during a viral infection: CD4 T cell responses are larger than we think. J Immunol. 2011;187(11):5568–5576. doi:10.4049/jimmunol.1102104.

37. Jian JY, Inoue SI, Bayarsaikhan G, Miyakoda M, Kimura D, Kimura K, Nozaki E, Sakurai T, Fernandez-Ruiz D, Heath WR. et al. CD49d marks Th1 and Tfh-like antigen-specific CD4+ T cells during plasmodium chabaudi infection. Int Immunol. 2021;33(8):409–422. doi:10.1093/intimm/dxab020.

38. Mo RR, Eisenbraun JK, Sonstein J, Craig RA, Curtis JL, Stoolman LM, Chen J, Yung RL. CD49d overexpression and T cell autoimmunity. J Immunol. 2003;171(2):745–753. doi:10.4049/jimmunol.171.2.745.

39. Berard M, Tough DF. Qualitative differences between naive and memory T cells. Immunology. 2002;106(2):127–138. doi:10.1046/j.1365-2567.2002.01447.x.

40. Peng H, He X, Wang Q. Immune checkpoint blockades in gynecological cancers: a review of clinical trials. Acta Obstet Gynecol Scand. 2022;101(9):941–951. doi:10.1111/aogs.14412.

41. Peng Z, Li M, Li H, Gao Q. PD-1/PD-L1 immune checkpoint blockade in ovarian cancer: dilemmas and opportunities. Drug Discov Today. 2023;28(8):103666. doi:10.1016/j.drudis.2023.103666.

42. Abdalla M, Aa E-A, Gai Z. CTLA-4 and ovarian cancer residual tumors: the dark side of debulking surgery. Hum Cell. 2023;36(6):2281–2283. doi:10.1007/s13577-023-00976-6.

43. Yin Q, Wu L, Han L, Zheng X, Tong R, Li L, Bai L, Bian Y. Immune-related adverse events of immune checkpoint inhibitors: a review. Front Immunol. 2023;14:1167975. doi:10.3389/fimmu.2023.1167975.

44. Lee DJ, Lee HJ Jr., Farmer JR, Reynolds KL. Mechanisms driving immune-related adverse events in cancer patients treated with immune checkpoint inhibitors. Curr Cardiol Rep. 2021;23(8):98. doi:10.1007/s11886-021-01530-2.

45. Zwanenburg ES, El Klaver C, Wisselink DD, Punt CJA, Snaebjornsson P, Crezee J, Aalbers AGJ, Brandt-Kerkhof ARM, Bremers AJA, Burger PJWA. et al. Adjuvant hyperthermic intra-peritoneal chemotherapy in patients with locally advanced colon cancer (COLOPEC): 5-year results of a randomized multicenter trial. J Clin Oncol. 2023;JCO2202644. 42(2):140–145. doi:10.1200/JCO.22.02644.

46. Donskov F, Xie W, Overby A, Wells JC, Fraccon AP, Sacco CS, Porta C, Stukalin I, Lee J-L, Koutsoukos K. et al. Synchronous versus metachronous metastatic disease: impact of time to metastasis on patient outcome—results from the international metastatic renal cell carcinoma database consortium. Eur Urol Oncol. 2020;3(4):530–539. doi:10.1016/j.euo.2020.01.001.

47. Thomas EM, Wright JA, Blake SJ, Page AJ, Worthley DL, Woods SL. Advancing translational research for colorectal immuno-oncology. Br J Cancer. 2023;129(9):1442–1450. doi:10.1038/s41416-023-02392-x.

48. Tamaki S, Suzuki K, Abe I, Endo Y, Kakizawa N, Watanabe F, Saito M, Tsujinaka S, Miyakura Y, Ohta S. et al. Overexpression of satellite RNAs in heterochromatin induces chromosomal instability and reflects drug sensitivity in mouse cancer cells. Sci Rep. 2022;12(1):10999. doi:10.1038/s41598-022-15071-3.

49. Meraz IM, Savage DJ, Segura-Ibarra V, Li J, Rhudy J, Gu J, Serda RE. Adjuvant cationic liposomes presenting MPL and IL-12 induce cell death, suppress tumor growth, and alter the cellular phenotype of tumors in a murine model of breast cancer. Mol Pharm. 2014;11(10):3484–3491. doi:10.1021/mp5002697.

50. Meraz IM, Melendez B, Gu J, Wong ST, Liu X, Andersson HA, Serda RE. Activation of the inflammasome and enhanced migration of microparticle-stimulated dendritic cells to the draining lymph node. Mol Pharm. 2012;9(7):2049–2062. doi:10.1021/mp3001292.

51. Sedlacek AL, Gerber SA, Randall TD, van Rooijen N, Frelinger JG, Lord EM. Generation of a dual-functioning antitumor immune response in the peritoneal cavity. Am J Pathol. 2013;183(4):1318–1328. doi:10.1016/j.ajpath.2013.06.030.